Hindawi Publishing Corporation
International Journal of Antennas and Propagation
Volume 2012, Article ID 829780, 9 pages
doi:10.1155/2012/829780

Research Article

Development of Full-Scale Ultrathin Shell Reflector

Durmuş Türkmen,[1] Ömer Soykasap,[2] and Şükrü Karakaya[3]

[1] *Department of Mechanical Engineering, Pamukkale University, 20070 Denizli, Turkey*
[2] *Department of Material Science and Engineering, Afyon Kocatepe University, 03200 Afyonkarahisar, Turkey*
[3] *Department of Mechanical Education, Afyon Kocatepe University, 03200 Afyonkarahisar, Turkey*

Correspondence should be addressed to Ömer Soykasap, soykasap@aku.edu.tr

Received 16 December 2011; Accepted 21 March 2012

Academic Editor: Carles Fernández-Prades

It is aimed that a new ultrathin shell composite reflector is developed considering different design options to optimize the stiffness/mass ratio, cost, and manufacturing. The reflector is an offset parabolic reflector with a diameter of 6 m, a focal length of 4.8 m, and an offset of 0.3 m and has the ability of folding and self-deploying. For Ku-band missions a full-scale offset parabolic reflector antenna is designed by considering different concepts of stiffening: (i) reflective surface and skirt, (ii) reflective surface and radial ribs, and (iii) reflective surface, skirt, and radial ribs. In a preliminary study, the options are modeled using ABAQUS finite element program and compared with respect to their mass, fundamental frequency, and thermal surface errors. It is found that the option of reflective surface and skirt is more advantageous. The option is further analyzed to optimize the stiffness/mass ratio considering the design parameters of material thickness, width of the skirt, and ply angles. Using the TOPSIS method is determined the best reflector concept among thirty different designs. Accordingly, new design can be said to have some advantages in terms of mass, natural frequency, number of parts, production, and assembly than both SSBR and AstroMesh reflectors.

1. Introduction

There have been extensive studies on spaceborne reflectors to increase the performance with a reduced cost. There are a number of reflector concepts; selection of the best concept depends on application and size of the reflectors. The main requirement for large reflectors is that they must be packaged in the limited volume of the launch vehicle, and they must be deployed to required shape in orbit. In order to compactly package a large reflector, the structure is to be folded or bent; the smaller packaged volume is required to lower the launch cost [1, 2]. Folding and self-deploying shell reflector has a thin reflective surface and some reinforcements to stiffen the structure, which are designed to allow folding [3]. Tan et al. studied the stiffened spring-back reflector (SSBR), showing the feasibility, folding, and self-deploying capability of a 0.8 scaled demonstrator. The full-size high-accuracy offset reflector of 6 m diameter met the requirements for Ku-band application [4]. Datashvili et al. studied the technical assessment of the high-accuracy large-spaceborne reflector antenna concepts for Ku-band. Thin shell reflector antenna (SSBR) was selected as one of the best options. The SSBR concept has several advantages over the current state-of-the-art AstroMesh reflector, namely, simplicity, relatively lower manufacturing costs, a lower surface error, and a simpler folding. On the other hand, the main advantages of AstroMesh are its lower mass and its small packaged volume [1, 5].

In this study, it is aimed that a new ultrathin shell composite reflector is developed considering different design options to optimize the stiffness/mass ratio, cost, and manufacturing. SSBR is taken as reference reflector with a diameter of $D = 6$ m, a focal length of $F = 4.8$ m, and an offset distance of 0.3 m. The concepts of stiffening the reflector structure include (i) reflective surface and skirt, (ii) reflective surface and radial ribs, and (iii) reflective surface, skirt, and radial ribs. In a preliminary study, the options are modeled using the ABAQUS finite element program [6] and compared in terms of their mass and fundamental frequencies. It is found the concept of reflective surface and skirt is more advantageous over the other options. The concept is further analyzed to optimize the stiffness/mass ratio considering the design parameters of thickness of the skirt, width of the skirt, and

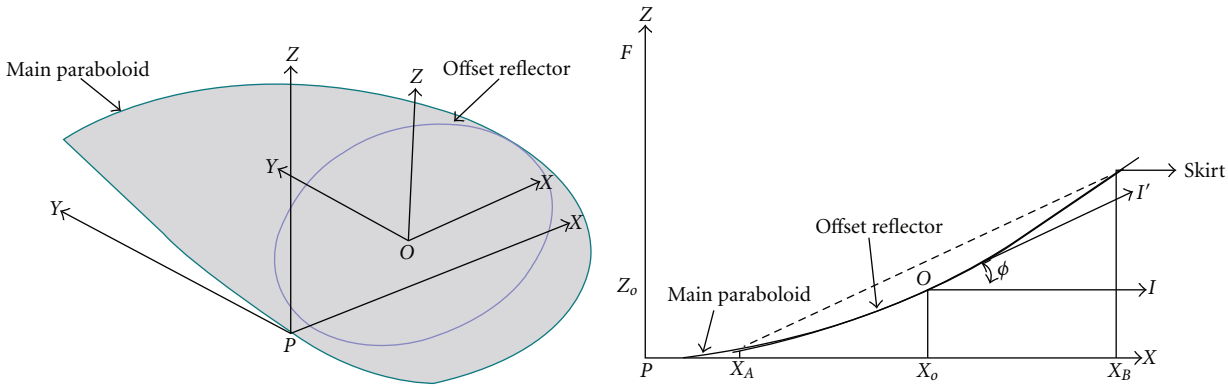

Figure 1: Offset reflector.

ply angles. Using the TOPSIS method will be determined the best reflector design among thirty different designs. Then, new design will be compared with SSBR and AstroMesh reflectors.

2. Preliminary Design

The full-scale reflector is an offset parabolic reflector with a diameter of $D = 6$ m, a focal length of $F = 4.8$ m, and an offset of $X_A = 0.3$ m. The reflector is modeled in the ABAQUS finite element software; first, the main paraboloid is created; next the offset reflector surface is obtained by a cut using a cylinder with its axis z being parallel to the axis Z of the paraboloid. Figure 1 shows the details of the modeling, where offset distance $X_A = 0.3$ m and diameter of the reflector $D = X_B - X_A = 6$ m. There is also flat skirt with a width of 0.15 m around the rim of the reflector. The SSBR used a triaxial carbon fiber/epoxy for the reflector, but there are thermal distortion problems in the triaxial material; hence, a plain weave carbon/epoxy is chosen instead for the new reflector. The reflector is assumed to be made of plain weave carbon T300B/L160 epoxy, with an areal density of dry cloth of 94 g/m^2 and a ply thickness of 0.11 mm. Material properties of a single ply are obtained for a fiber volume fraction of $V_f = 0.485$ as $E_1 = E_2 = 60.2$ GPa, $G_{12} = 2.94$ GPa, $\nu_{12} = 0.031$, and $\rho = 1.440$ kg/m^3, which is based on the analytical approach developed for plain-woven composite materials [7].

The three concepts of stiffening the reflector structure include (i) reflective surface and skirt, (ii) reflective surface and radial ribs, and (iii) reflective surface, skirt, and radial ribs. The reflector surface is modeled as a laminated composite shell, using *S4R* quadratic elements, with a total number of elements of 14250. The concepts are compared in terms of mass and fundamental frequency.

2.1. The Concept of Reflective Surface and Skirt. It is envisaged that a reflector with much simpler design and significantly lower mass and lower cost is possible by considering some design changes on SSBR. First, several stiffening elements including radial, spiral, central, and rim reinforcements and a skirt were used in the original SSBR. All reinforcing

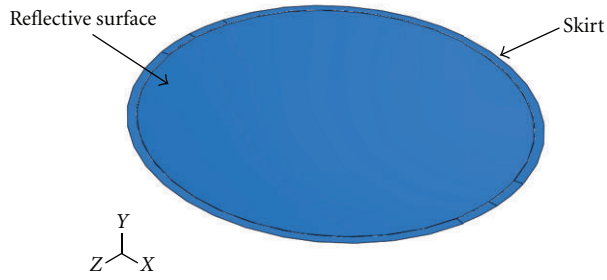

Figure 2: Reflective surface with flat skirt, case E.

elements except the skirt are removed in the new reflector in order to simplify the structure and to reduce its mass. Second, there were circumferential slits on the skirt near the rim that was introduced to reduce the stress and/or strain in the structure during folding. All slits are removed in the new concept. Hence, we consider only reflective surface with a flat skirt to investigate full advantage of stiffening.

The concept is modeled in ABAQUS as seen in Figure 2. It consists of two parts: reflective surface and skirt that are connected to each other by tie constraints. The skirt is made of three plies (0/45/0) and a width of 0.15 m, whereas the reflective surface is made of either three plies (0/45/0) or two plies (0/45). The case of reflective surface and skirt is denoted as case E.

2.2. The Concept of Reflective Surface and Rib. Composite tape springs are commonly used for deployable structures for stiffening the structure. The tape springs exhibit high initial stiffness in deployed configuration and folds and deploys elastically (can be seen in Figure 7).

Therefore, it can be a good choice to stiffen the reflective surface as a rib. Figures 3 and 4 show the modeled reflector with initially curved large tape springs. Two options are considered: (i) the tape springs are attached to the back of the reflective surface and subject to opposite sense bending during folding of the reflector denoted as case T and (ii) the tape springs are attached to the back of the reflective surface and subject to equal sense bending during folding of

Table 1: Comparison of different design cases.

Designs	Frequency, (Hz)								mass (kg)
	Mode 1	Mode 2	Mode 3	Mode 4	Mode 5	Mode 6	Mode 7	Mode 8	
case E[a]	1.025	1.124	3.362	3.385	6.735	6.775	9.282	9.734	15.91
case E[b]	**1.110**	**1.212**	**3.632**	**3.654**	**6.920**	**6.942**	**7.712**	**7.725**	**11.08**
case T[a]	0.254	0.274	0.328	0.395	0.407	1.018	1.092	1.097	17.69
case T[b]	0.232	0.277	0.295	0.351	0.356	0.796	0.905	1.065	12.86
case D[a]	1.515	1.536	2.262	2.475	2.605	3.251	3.612	3.674	17.69
case D[b]	**1.448**	**1.461**	**2.078**	**2.290**	**2.328**	**2.681**	**2.865**	**2.914**	**12.86**
case ET[a]	1.102	1.190	3.516	3.531	6.789	7.145	9.680	9.796	19.15
case ET[b]	1.178	1.260	3.712	3.722	6.925	7.353	8.288	8.479	14.32
case ED[a]	2.254	2.314	5.077	5.089	8.306	8.476	9.990	10.18	19.15
case ED[b]	**2.293**	**2.342**	**5.160**	**5.182**	**7.972**	**8.136**	**8.426**	**8.635**	**14.32**

[a]: reflective surface with three plies, [b]: reflective surface with two plies.

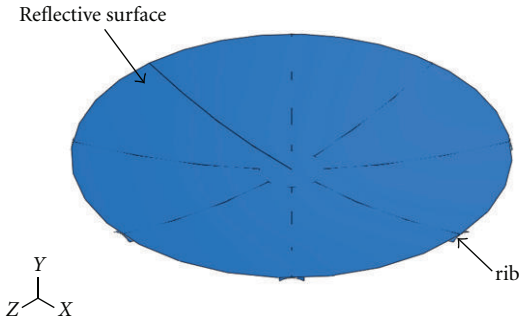

Figure 3: Reflective surface with tape springs, case T.

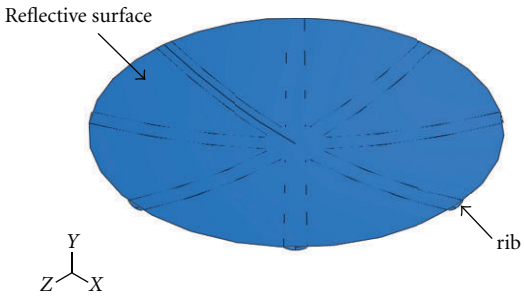

Figure 4: Reflective surface with tape spring, case D.

the reflector denoted as case D. For case T, the tape springs have the same longitudinal curvature as the reflective surface and are connected to the reflective surface tangentially. For case D, the tape springs have the same longitudinal curvature as the reflective surface, but are connected to the reflective surface through their edges. For both cases, eight tape springs are considered and connected to reflective surface by tie constraints. The tape springs have a subtended angle of 60 deg and transverse radius of 0.3 m and are made of three ply (0/45/0) composites of the same material. Again the reflective surface is assumed to be made of either three plies (0/45/0) or two plies (0/45).

2.3. Concept of Reflective Surface with Skirt and Ribs. In this concept the reflective surface is stiffened by both skirt and ribs. Flat skirt is added to the models shown in Figures 3 and 4 by tie constraints. The skirt and ribs are assumed to have three plies (0/45/0). The cases of reflective surface with skirt and ribs are denoted as case ED and case ET.

2.4. Results of Preliminary Analysis. The modal analysis is carried out for each reflector under free boundary conditions; the natural frequencies, mass, and the mode shapes are obtained. The results are given in Table 1. The cases of E, D, and ED with reflective surface of two plies are better when high fundamental frequency with low mass is considered. The reflective surface with two plies is advantageous due to less thickness and material cost.

The reflective surface with skirt, case E, has the lowest mass, and it also satisfies the requirement of a minimum fundamental frequency of 1 Hz. It can be manufactured as a single piece. It allows folding and self-deploying. Hence, it is the best option compared to the other cases.

The reflective surface with rib, case D, has a slightly higher mass and a higher fundamental frequency. However, the other modes except mode two have less natural frequencies than that of case E. The reflective surface and the ribs must be manufactured separately. Attachment of the ribs to the reflective surface is another issue that must be further studied. 3D folding behavior of the ribs or the reflective surface with ribs should be investigated.

The reflective surface with skirt and ribs, case ED, has the highest fundamental frequency but with a higher mass. This makes manufacturing even more difficult, and it has still the same drawbacks of case D.

The mode shapes of the options are given in Figure 5. In all cases mode shapes have circumferential sine waves along the rim of the reflector. Two consecutive natural frequencies are close to each other; corresponding modes are similar but with a phase angle.

2.5. Thermal Analysis. Structural parts that work in space environment are subject to great temperature variance. So, the structural parts need to be made of materials with low

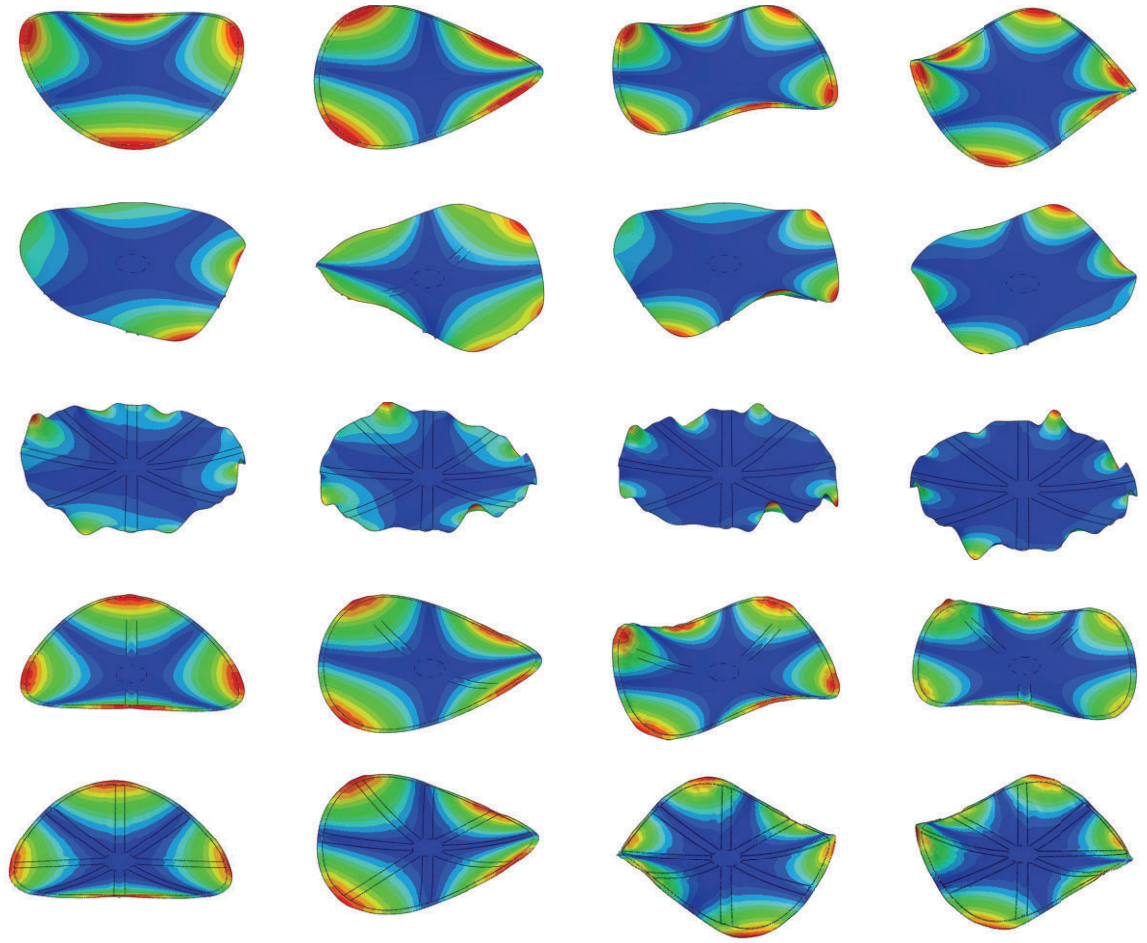

Figure 5: First four modes of the cases E, T, D, ET, and ED with three-ply reflective surface, from top to down.

coefficient of thermal expansion (CTE). Thermal changes that occur in orbit cause surface errors and reductions in performance. Thermal analysis is carried out under thermal loads for the best three designs of case E^b, case D^b, and case ED^b, and then the surface error is estimated, which can be used to estimate the electrical performance. In order to measure the surface accuracy, root mean square error (RMS) is considered. The surface accuracy of reflective surface can be obtained by considering the ideal design surface and the best-fit paraboloid surface. The best-fit paraboloid is defined in XYZ coordinate system as $Z = (X^2 + Y^2)/(4F)$, and it is obtained by minimizing the RMS error using parameters of Euler rotation angles (θ, ϕ, φ) and the parameters of translations (x_0, y_0, z_0) from the xyz coordinate system as follows:

$$\begin{bmatrix} X \\ Y \\ Z \end{bmatrix} = BCD \begin{bmatrix} x \\ y \\ z \end{bmatrix} + \begin{bmatrix} x_0 \\ y_0 \\ z_0 \end{bmatrix},$$

$$B = \begin{bmatrix} \cos(\psi) & \sin(\psi) & 0 \\ -\sin(\psi) & \cos(\psi) & 0 \\ 0 & 0 & 1 \end{bmatrix},$$

$$C = \begin{bmatrix} 1 & 0 & 0 \\ 0 & \cos(\theta) & \sin(\theta) \\ 0 & -\sin(\theta) & \cos(\theta) \end{bmatrix},$$

$$D = \begin{bmatrix} \cos(\phi) & \sin(\phi) & 0 \\ -\sin(\phi) & \cos(\phi) & 0 \\ 0 & 0 & 1 \end{bmatrix}. \tag{1}$$

RMS error in Z direction is calculated for all the nodes as follows:

$$\delta_{\text{rms}} = \sqrt{\frac{\sum \left(\hat{Z}_i - Z_i\right)^2}{n}}, \tag{2}$$

where $\hat{Z}_i$ is the coordinate of a point of distorted surface and Z_i is the corresponding coordinate of the best-fit paraboloid.

The woven carbon/epoxy composite, which is used for the reflective surface and the ribs, has a CTE of between $2 \times 10^{-6}/^\circ\text{C}$ and $6 \times 10^{-6}/^\circ\text{C}$. However, a lower CTE is obtained when special resin for the space applications is used; hence a CTE of $0.5 \times 10^{-6}/^\circ\text{C}$ is taken for the analysis. Thermal

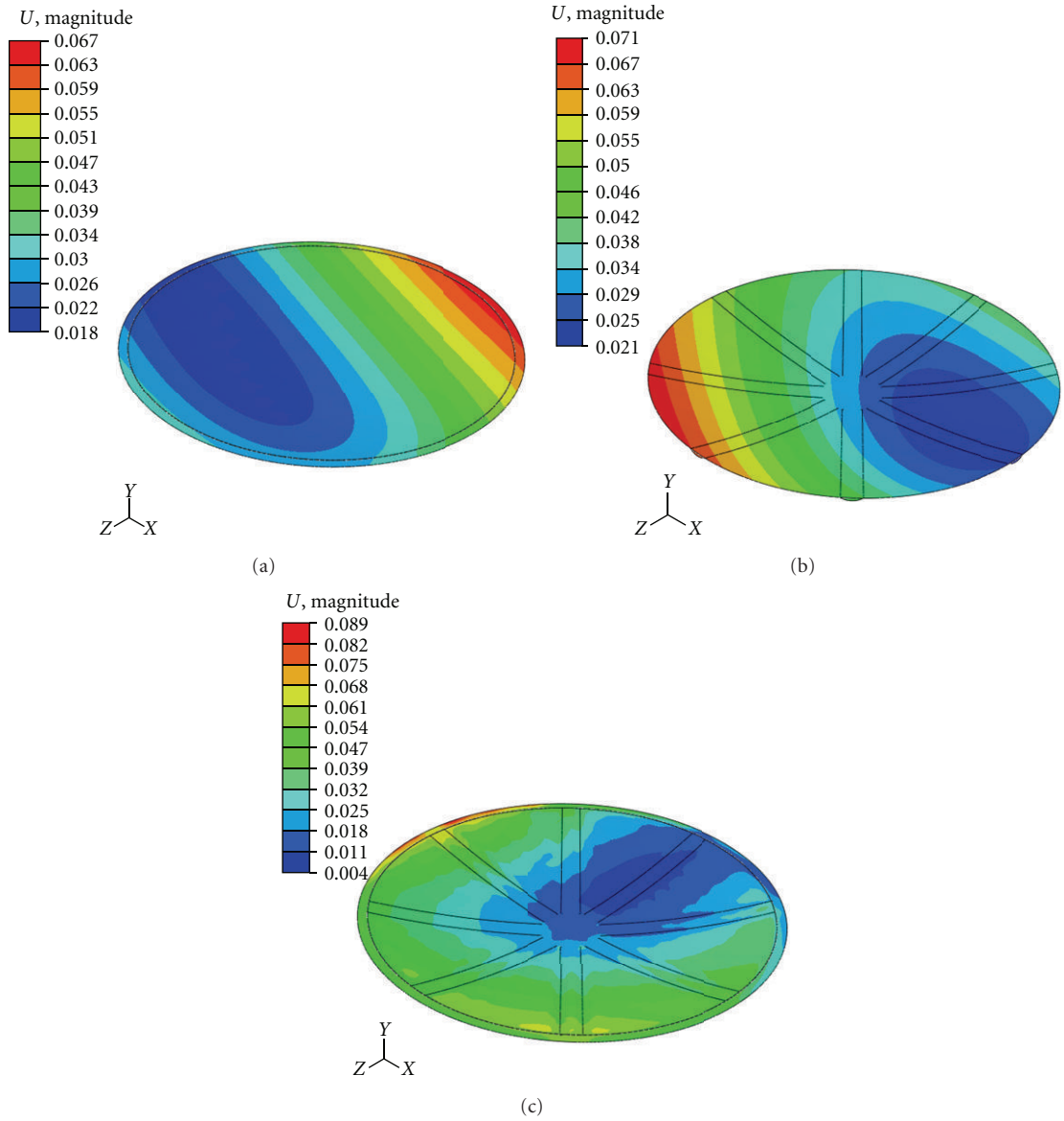

Figure 6: Displacement magnitudes due to LC3 thermal loading (units in mm), case E^b (a), case D^b, (b), and case ED^b (c).

Table 2: RMS errors for thermal loads.

Thermal loads	E^b		D^b		ED^b	
	RMS (mm)	F (mm)	RMS (mm)	F (mm)	RMS (mm)	F (mm)
LC1	0.003	4800.25	0.06	4800.36	0.045	4800.16
LC2	0.050	4802.52	0.08	4800.75	0.055	4800.90
LC3	0.035	4800.40	0.04	4800.20	0.032	4800.25

loading conditions are as follows [1, 8]:

LC1: a gradient along the x-direction of 100°C over the total length of the reflector,

LC2: uniform absolute temperature −150°C,

LC3: uniform absolute temperature 170°C.

The thermal loads are applied to the finite element model of three concepts using initial temperature of 20°C. The displacement contours are shown in Figure 6 for each concept. The focal length and RMS error for each concept are given in Table 2. The worst loading is LC2 for both RMS and the focal length. All concepts yield similar results of

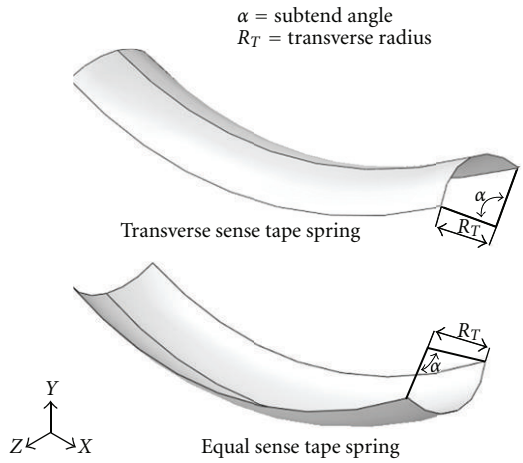

Figure 7

a low RMS error and small variation in the design focal length; hence they all are acceptable.

3. Optimization of the Reflector with Skirt

The preliminary study showed that the option of reflective surface with skirt suits better for low cost, low mass, and sufficient stiffness. Therefore, it is chosen as the best concept for the new thin shell reflector. In order to increase stiffness while keeping low mass the structure is optimized considering design changes. During the optimization the following is considered for the design. First the reflective surface is to have a continuous surface; no discontinuity is allowed. Next the reflector mass should be less than 14 kg. Then the reflector has the minimum number of parts with manufacturing ease and low cost. Last but not least the reflector must be foldable.

The design parameters are the thickness of the skirt, t_2, width of the skirt, w, and composite ply angles of the skirt. Three different widths, 150 mm, 200 mm, and 250 mm, for the skirt and a maximum of six plies for the skirt are considered. The reflective surface has the plies 0/45 with a thickness of 0.22 mm, which are taken to be constant. The mass and fundamental frequencies are given in Table 3.

Adding 45 deg plies to the skirt increases the frequency. Increasing the width of the skirt increases both the mass and the frequency of the structure. The design with a skirt of 0/45/45/0 and a width of 250 mm has the highest frequency/mass ratio. However, the frequency is not critical; the design with a skirt of 0/45/0 and a width of 250 mm has the second highest frequency/mass ratio but has a lower mass and frequency.

3.1. Determination of the Best Offset Reflector Model Using TOPSIS Method. The TOPSIS method developed by Hwang and Yoon is one of the multicriteria decision-making techniques. The basis of the method is the decision points based on the proximity of the ideal solution. With this method, the maximum and minimum values can be compared to the ideal state [9–13]. The TOPSIS method consists of six steps. The TOPSIS method steps are described below.

Table 3: Comparison of different designs of reflective surface with skirt.

Design no.				
	Skirt with plies 0_n, w = 150 mm			
	n	t_2 (mm)	mass (kg)	Freq. (Hz)
1	2	0.22	10.600	0.768
2	3	0.33	11.085	0.850
3	4	0.44	11.550	0.912
4	5	0.55	12.020	0.954
5	6	0.66	12.500	0.988
	Skirt with plies 0_n, w = 200 mm			
	n	t_2 (mm)	mass (kg)	Freq. (Hz)
6	2	0.22	10.930	1.025
7	3	0.33	11.560	1.127
8	4	0.44	12.200	1.199
9	5	0.55	12.840	1.245
10	6	0.66	13.475	1.278
	Skirt with plies 0_n, w = 250 mm			
	n	t_2 (mm)	mass (kg)	Freq. (Hz)
11	2	0.22	11.260	1.330
12	3	0.33	12.060	1.469
13	4	0.44	12.860	1.533
14	5	0.55	13.660	1.569
15	6	0.66	14.460	1.585
	Skirt with plies $0/45_n/0$, w = 150 mm			
	n	t_2 (mm)	mass (kg)	Freq. (Hz)
16	0	0.22	10.600	1.070
17	1	0.33	11.085	1.195
18	2	0.44	11.550	1.350
19	3	0.55	12.020	1.388
20	4	0.66	12.500	1.399
	Skirt with plies $0/45_n/0$, w = 200 mm			
	n	t_2 (mm)	mass (kg)	Freq. (Hz)
21	0	0.22	10.930	1.470
22	1	0.33	11.560	1.620
23	2	0.44	12.200	1.829
24	3	0.55	12.840	1.851
25	4	0.66	13.475	1.852
	Skirt with plies $0/45_n/0$, w = 250 mm			
	n	t_2 (mm)	mass (kg)	Freq. (Hz)
26	0	0.22	11.260	1.702
27	1	0.33	12.060	1.990
28	2	0.44	12.860	2.145
29	3	0.55	13.660	2.135
30	4	0.66	14.460	2.105

Table 4: Reflector designs.

Weight coefficients	w_1	w_2	w_3	w_4	Value of proximity to decision C_i^*
Designs	Mass, (kg)	Fundamental frequency (Hz)	Manufacturing cost	Packing volume	
1	10.60	0.768	1	5	0.405
2	11.08	0.850	2	4	0.355
3	11.55	0.912	3	3	0.286
4	12.02	0.954	4	2	0.223
5	12.50	0.988	5	1	0.214
6	10.93	1.025	1	5	0.458
7	11.56	1.127	2	4	0.430
8	12.20	1.199	3	3	0.388
9	12.84	1.245	4	2	0.351
10	13.47	1.278	5	1	0.340
11	11.26	1.330	1	5	0.549
12	12.06	1.469	2	4	0.564
13	12.86	1.533	3	3	0.539
14	13.66	1.569	4	2	0.498
15	14.46	1.585	5	1	0.464
16	10.60	1.070	1	5	0.465
17	11.08	1.195	2	4	0.444
18	11.55	1.350	3	3	0.435
19	12.02	1.388	4	2	0.391
20	12.50	1.399	5	1	0.361
21	10.93	1.470	1	5	0.587
22	11.56	1.620	2	4	0.612
23	12.20	1.829	3	3	0.636
24	12.84	1.851	4	2	0.578
25	13.47	1.852	5	1	0.525
26	**11.26**	**1.702**	**1**	**5**	**0.672**
27	**12.06**	**1.990**	**2**	**4**	**0.750**
28	**12.86**	**2.145**	**3**	**3**	**0.725**
29	13.66	2.135	4	2	0.654
30	14.46	2.105	5	1	0.588

Step 1 (creating the decision matrix). The decision matrix consists of rows of decision point located in the lines. Factors in the evaluation takes place in the columns. The decision matrix is shown as follows:

$$A_{ij} = \begin{bmatrix} a_{11} & a_{12} & \cdots & a_{1n} \\ a_{21} & a_{22} & \cdots & a_{2n} \\ \vdots & & & \vdots \\ a_{m1} & a_{m2} & \cdots & a_{mn} \end{bmatrix}, \quad (3)$$

A_{ij} is the matrix, m the number of decision point, and n the number of assessment factor.

Step 2 (creating standard decision matrix (R)). Standard decision matrix is calculated using the following formula:

$$r_{ij} = \frac{a_{ij}}{\sqrt{\sum_{k=1}^{m} a_{kj}^2}}. \quad (4)$$

Thus, the R matrix is obtained as follows:

$$R_{ij} = \begin{bmatrix} r_{11} & r_{12} & \ldots & r_{1n} \\ r_{21} & r_{22} & \ldots & r_{2n} \\ \vdots & & & \vdots \\ r_{m1} & r_{m2} & \ldots & r_{mn} \end{bmatrix}. \quad (5)$$

Step 3 (constructing the weighted normalized decision matrix (V)). Weight values are determined according to

Table 5: Comparison of new design, SSBR, and AstroMesh.

	New Design	SSBR [1–4]	AstroMesh [15]
Aperture Diameter, m	6	6	6
F/D	0.8	0.8	0.64
Offset, m	0.3	0.3	0.75
Mass, kg	12.06	23.6	14.50
Fundamental frequency, Hz	1.99	1.87	2.00
Number of parts	Monolithic	Monolithic	Many (nets, meshes, ring truss, etc.)
Manufacturing and assembly	Easier	Easy	Difficult

purpose ($\omega ij : i : 1, 2, \ldots N$). Then each column of the R matrix elements multiplying with ωij value and V matrix is created:

$$V_{ij} = \begin{bmatrix} w_1 r_{11} & w_2 r_{12} & \ldots & w_n r_{1n} \\ w_1 r_{21} & w_2 r_{22} & \ldots & w_n r_{2n} \\ \vdots & & & \vdots \\ w_1 r_{m1} & w_2 r_{m2} & \ldots & w_n r_{mn} \end{bmatrix}. \quad (6)$$

Step 4 (ideal (A^*) and negative ideal (A^-) creating solutions). For creating the ideal solution set, the elders of column values of V matrix are selected. Finding the ideal solution set is shown in the following formula:

$$A^* = \left\{ \left(\max_i v_{ij} \mid j \in J \right), \left(\min_i v_{ij} \mid j \in J' \right) \right\}. \quad (7)$$

Here, $A^* = \{v_1^*, v_2^*, \ldots, v_n^*\}$ and J is maximization and J' minimization of the value negative ideal.

For creating the negative ideal solution set, the smaller of column values of V matrix are selected. Finding the negative ideal solution set is shown in the following formula:

$$A^- = \left\{ \left(\min_i v_{ij} \mid j \in J \right), \left(\max_i v_{ij} \mid j \in J' \right) \right\}. \quad (8)$$

Here, $A^- = \{v_1^-, v_2^-, \ldots, v_n^-\}$ is shown.

Step 5 (calculating the separation measure). For finding the deviations of solution set the Euclidian distance approach is utilized. Here, the obtained deviation values are called ideal (S_i^*) and negative ideal separation (S_i^-) measures. Ideal and negative ideal separation are calculated using the following formula:

$$S_i^* = \sqrt{\sum_{j=1}^{n} (v_{ij} - v_j^*)^2}, \qquad S_i^- = \sqrt{\sum_{j=1}^{n} (v_{ij} - v_j^-)^2}. \quad (9)$$

Step 6 (calculating the relative closeness for the ideal solution). To calculate the ideal solution proximity (C_i^*), the ideal and negative ideal separation measure is used. Calculation of the relative proximity to the ideal solution is shown in the following formula:

$$C_i^* = \frac{S_i^-}{S_i^- + S_i^*}. \quad (10)$$

Here, C_i^* value gets the range of $0 \le C_i^* \le 1$ [14].

3.2. Determining the Best Reflector Design. The natural frequency and mass constitute the first two-column decision matrix of values in Table 4. The other two columns are manufacturing costs and packaging volume. While skirt thickness and skirt width increase, the manufacturing cost increases. The same situation is valid for packing volume. The package volume increases with the skirt thickness. This is due to the fact that the minimum bend radius increases with the thickness of material. For these reasons, these criteria are taken into account using scores from 1 to 5. Weight coefficients of decision matrix are determined as $w_1 = 0.4$, $w_2 = 0.35$, $w_3 = 0.05$, and $w_4 = 0.20$.

The decision-making process is evaluated with the TOPSIS method by taking into account four different criteria and thirty different designs. Value of proximity to decision is seen in Table 4. The ideal design is obtained when value of proximity to decision is the highest. According to this, the best design is the twenty-seventh design. The optimized results are compared with SSBR and Astromesh reflector as given in Table 5. The new design has some advantages in terms of lower mass, number of parts, ease of manufacturing and assembly. The 1/3 scale predesign reflector is accomplished and a part of ground tests such as folding, modal, and deploying have been completed. Predesign reflector made of three-ply (0/45/0) plain weave carbon/epoxy can be seen in Figure 8.

4. Conclusions

A new ultrathin shell composite reflector is developed considering different design options to optimize the stiffness/mass ratio, cost, and manufacturing. The stiffened spring-back reflector is taken as reference reflector. Preliminary design study shows that the reflective surface with only a skirt has simpler design with high stiffness/mass ratio. This option is further analyzed to optimize the stiffness/mass ratio

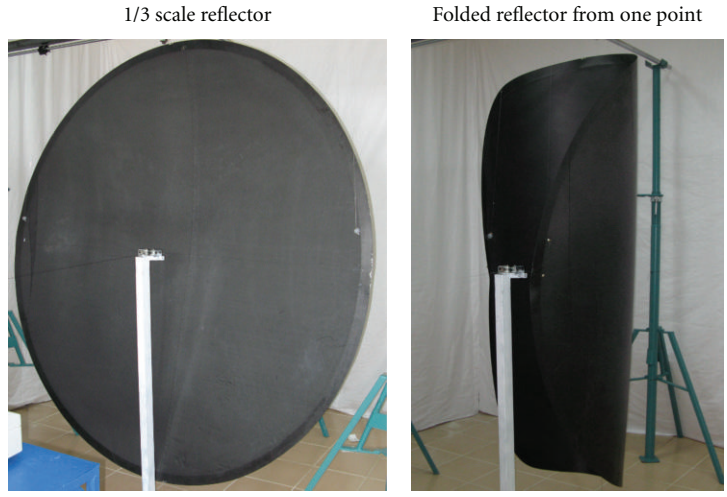

Figure 8

considering the design parameters of material thickness, width of the skirt, and ply angles. The optimized reflector has a mass of 12.06 kg and a fundamental frequency of 1.99 Hz. The new design has some advantages compared with previous design of both the stiffened spring-back reflector and AstroMesh reflector.

Acknowledgments

This research work is supported by the Scientific and Technological Research Council of Turkey under Grant 109M421 and the Pamukkale University Scientific Research Center.

References

[1] Ö. Soykasap and L. T. Tan, "High-precision offset stiffened springback composite reflectors," *AIAA Journal*, vol. 49, no. 10, p. 2144, 2011.

[2] Ö. Soykasap, A. Watt, S. Pellegrino, and P. Howard, "Novel concept for all-composite deployable SAR reflectors," in *Proceedings of the European Conference on Spacecraft Structures, Materials & Mechanical Testing (ESA/ESTEC '05)*, Noordwijk, The Netherlands, 2005.

[3] Ö. Soykasap and S. Karakaya, "Design of folding and self-deploying thin shell reflector," in *Proceedings of the International Scientific Conference on Advanced Lightweight Structures and Reflector Antennas*, Tbilisi, Ga, USA, October 2009.

[4] L. T. Tan, Ö. Soykasap, and S. Pellegrino, "Design & manufacture of stiffened spring-back reflector demonstrator," in *Proceedings of the 46th AIAA/ASME/ASCE/AHS/ASC Structures, Structural Dynamics and Materials Conference*, AIAA Paper 2005–2048, pp. 3078–3088, Austin, Tex, USA, April 2005.

[5] L. Datashvili, M. Lang, C. Zauner et al., "Technical assessment of high accuracy large space borne reflector antenna (TAHARA)," Tech. Rep. number TR LLB-R-12/07/04-02D-02, Technical University of Munich, Munich, Germany, 2004.

[6] "ABAQUS/Standard User's Manual," Ver. 6.10, Dassault Systèmes Simulia Corp., Pawtucket, RI, USA, 2010.

[7] Ö. Soykasap, "Analysis of plain-weave composites," *Mechanics of Composite Materials*, vol. 47, no. 2, pp. 161–176, 2011.

[8] Y. Gowayed, W. Zou, and S. Gross, "Analytical approach to evaluate the coefficients of thermal expansion of textile composite materials," *Polymer Composites*, vol. 21, no. 5, pp. 814–820, 2000.

[9] P. Liu, "An extended TOPSIS method for multiple attribute group decision making based on generalized interval-valued trapezoidal fuzzy numbers," *Informatica*, vol. 35, no. 2, pp. 185–196, 2011.

[10] G. R. Jahanshahloo, F. H. Lotfi, and M. Izadikhah, "Extension of the TOPSIS method for decision-making problems with fuzzy data," *Applied Mathematics and Computation*, vol. 181, no. 2, pp. 1544–1551, 2006.

[11] F. Ecer, "Bulanık Ortamlarda Grup Kararı Vermeye Yardımcı Bir Yöntem Fuzzy TOPSIS Ve Bir Uygulama," *Dokuz Eylül Üniversitesi, İşletme Fakültesi Dergisi*, vol. 7, no. 2, pp. 77–96, 2006.

[12] J. Dodangeh, R. B. M. Yusuff, and J. Jassbi, "Using topsis method with goal programming for best selection of strategic plans in BSC model," *Journal of American Science*, vol. 6, no. 3, 2010.

[13] O. Jadidi, F Firouzi, and E. Bagliery, "TOPSIS method for supplier selection problem," *World Academy of Science, Engineering and Technology*, vol. 71, 2010.

[14] http://www.deu.edu.tr/userweb/k.yaralioglu/dosyalar/TOPSIS_Yontemi.doc.

[15] "AstroMesh Reflector," Document No. DS-409, Astro Aerospace, Redondo Beach, Calif, USA, 2004.